Self-catalyzed, pure zincblende GaAs nanowires grown on Si(111) by molecular beam epitaxy

G. E. Cirlin,[1,2,3,*] V. G. Dubrovskii,[1,2] Yu. B. Samsonenko,[1,2,3] A. D. Bouravleuv,[1,2] K. Durose,[4] Y. Y. Proskuryakov,[4] Budhikar Mendes,[4] L. Bowen,[4] M. A. Kaliteevski,[4] R. A. Abram,[4] and Dagou Zeze[4]

[1]*St.-Petersburg Academic University—Nanotechnology Research and Education Centre, Russian Academy of Sciences, Khlopina 8/3, 194021 St.-Petersburg, Russia*

[2]*Ioffe Physical Technical Institute, Russian Academy of Sciences, Politekhnicheskaya 26, 194021 St.-Petersburg, Russia*

[3]*Institute for Analytical Instrumentation, Russian Academy of Sciences, Rizhsky 26, 190103 St.-Petersburg, Russia*

[4]*Department of Physics, Durham University, South Road, Durham DH1 3BH, United Kingdom*

(Received 11 May 2010; revised manuscript received 11 June 2010; published 2 July 2010)

We report on the Au-free molecular beam epitaxy growth of coherent GaAs nanowires directly on Si(111) substrates. The growth is catalyzed by liquid Ga droplets formed in the openings of a native oxide layer at the initial growth stage. Transmission electron microscopy studies demonstrate that the nanowires are single crystals having the zincblende structure along their length (apart from a thin wurtzite region directly below the Ga droplet), regardless of their diameter (70–80 nm) and the growth temperature range (560–630 °C). We attribute the observed phase purity to a much lower surface energy of liquid Ga than that of Au-Ga alloys, which makes triple line nucleation energetically unfavorable. The change in growth catalyst to a liquid metal with a lower energy suppresses the (more usual) formation of wurtzite nuclei on surface energetic grounds. These results can provide a distinct method for the fabrication of chemically pure and stacking-fault-free zincblende nanowires of III-V compounds on silicon.

DOI: 10.1103/PhysRevB.82.035302 PACS number(s): 61.46.Km, 61.72.uj, 68.55.A−

I. INTRODUCTION

Nanowires (NWs) fabricated in a bottom-up manner[1,2] via the vapor-liquid-solid (VLS) mechanism[3] with a metallic (Au) catalyst have recently shown the ability to accumulate strain in two dimensions (2D) and to enable coherent growth at sufficiently small footprints.[4–6] The critical diameter for coherent epitaxial growth of NWs decreases with the lattice mismatch ε_0 (Ref. 4) and equals 24–26 nm for InAs/Si (ε_0 =11.6%), 36–38 nm for InP/Si (ε_0=8.1%), and 110 nm for GaAs/Si (ε_0=4.0%) systems.[5,6] The NW geometry therefore looks very promising for monolithic integration of III-V compounds on silicon. The controlled production of III-V NWs (in general, not only on Si substrates) requires, however, careful considerations of their chemical purity and crystal structure. Au-assisted VLS growth can lead to an unintentional Au contamination.[7] As regards the crystal-phase purity, it is now generally recognized that, in contrast to their bulk zincblende (ZB) form, most of III-V NWs tend to adopt hexagonal wurtzite (WZ) structure.[5,8–12] Usually, the WZ phase is not stable; the NWs have a disordered polytypelike structure with mixed WZ-ZB character. Since these stacking faults introduce unwanted defects, the control over the phase purity is now considered as one of the major challenges in NW fabrication techniques.

According to Ref. 13, the difference in bulk cohesive energies between the WZ and ZB GaAs phases amounts to 24 meV per pair. To overcome this difference and obtain WZ GaAs in bulk form, one should apply a huge pressure on the order of several tens of gigapascal.[14] In the NW geometry, the volume contribution to the overall formation enthalpy can be more than compensated by the surface-energy gain. Indeed, WZ NWs feature a lower number of dangling bonds on relevant sidewall facets and on the edges separating the facets.[15–17] A kinetic model of NW growth and crystal phase pioneered in Ref. 18 and further developed in Refs. 19 and 20 shows the importance of nucleation. During the mononuclear VLS growth of a NW, the WZ phase is favored if the nucleation barrier of 2D WZ island formation is lower than of a ZB one. This requires two conditions:[18] (i) the material-related condition for the surface energies to allow triple phase line (TL) nucleation (where some part of nucleus perimeter is in contact with the vapor and the lower surface energy of WZ sidewall facets can decrease the nucleation barrier) and (ii) a growth-related condition which makes liquid supersaturation decisive for the observed crystal structure. Also, increasing the NW diameter must suppress the TL nucleation[19] in the polynuclear growth mode and therefore restore the bulk ZB phase.

With these considerations, one method for tuning the crystal structure of III-V NWs is changing the deposition conditions and Au nanoparticle diameter.[21–27] For example, as demonstrated in Refs. 21 and 22 in the case of Au-assisted molecular beam epitaxy (MBE) of GaAs NWs on the GaAs substrates, intelligent manipulations of the growth conditions permit continuously low supersaturation in the vicinity of growing NWs and, consequently, the stacking-fault-free ZB structure. The study in Refs. 23 and 24 indicates that the structure of InAs and InP NWs can be controlled by the diameter and growth temperature. As expected, NWs of smaller diameter are predominantly WZ, with a temperature-dependent crossover to the ZB structure for larger diameters. In Ref. 25, the pure ZB phase in different III-V NWs grown by Au-catalyzed molecular-organic chemical-vapor deposition (MOCVD) is achieved using a low growth temperature coupled with a high V/III ratio. The comprehensive analysis in Ref. 27 confirms the pure ZB phase (regardless of NW diameter and the substrate material) only for antimonides. In the MOCVD case, liquid supersaturation during the NW growth is sensitive to the temperature-dependent pyrolysis efficiencies and therefore to the precursors used. This could

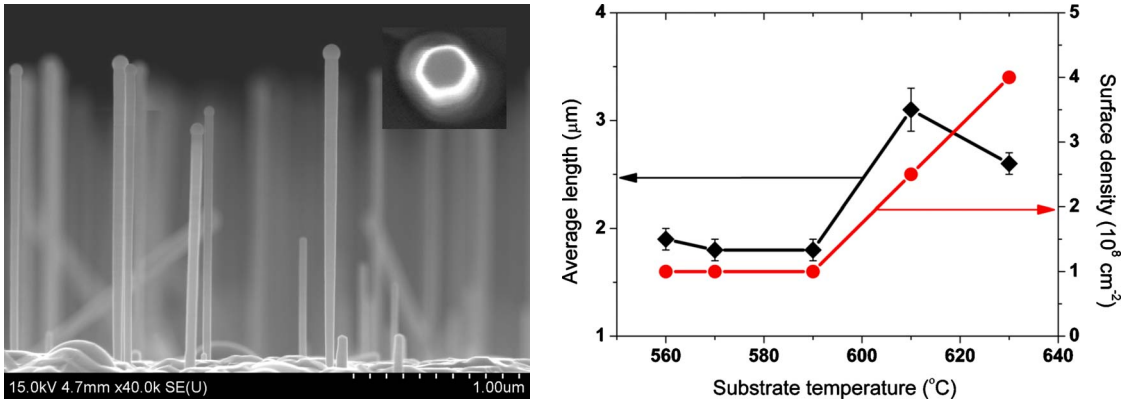

FIG. 1. (Color online) (a) Lateral cross-section view SEM image of GaAs NWs on Si(111) substrate grown at 590 °C, the inset shows the hexagonal NW cross section ; (b) the substrate temperature dependences of the average length and surface density of Ga-catalyzed NWs.

be an explanation of the controversial results of Ref. 5 that report the pure WZ structure for different III-V NWs and Ref. 27, where GaAs NWs appear to be pure ZB.

As regards the crystal structure of III-V NWs grown on Si substrates, the pure ZB phase has been observed in the case of Au-catalyzed MOCVD of GaAs NWs on the Si(111) substrates with AlGaAs buffers.[28] In Ref. 29, pure ZB, Ga-catalyzed GaAs NWs (although containing two twin ZB orientations) has been obtained by MBE on the GaAs substrates coated with a sputtered silicon dioxide layer. This study demonstrates the importance of As flux: ZB structure has been achieved only under sufficiently high As pressure. Self-assembled GaAs NWs of Ref. 30 could nucleate only on the (110) facets. Structural analysis demonstrated two types of NWs, the first one being terminated by a Ga droplet and the second by pyramidal shaped GaAs. The first type of NWs comprises the WZ phase remote from the droplet while the second type comprise predominantly ZB lattice with rather narrow WZ regions. Catalyst-free InAs NWs,[31] grown by MOCVD directly on Si(111) substrates, are mainly ZB, however, high densities of twins and stacking faults are found. In Ref. 32, epitaxial GaAs NWs were obtained by Au-assisted MBE on Si(100) and Si(111) substrates but the structural characterization again revealed mixed ZB/WZ character.

In this work, we present pure ZB NWs (excluding the very tips just beneath the Ga droplet, where stacking faults and WZ phase exist) grown directly on Si(111) substrate by a special MBE procedure. As in Ref. 29, the key point is the formation of liquid Ga nanoparticles at the initial stage in the openings of a native oxide layer but on the Si(111) substrate. These Ga droplets act as the catalyst seeds promoting NW nucleation via the VLS mechanism at the follow-up growth stage. It is demonstrated that the change in catalyst from Au to Ga has a tremendous effect on the crystal phase, which is found to be almost single-crystalline ZB. A simple nucleation model is used to explain the observed phase purity by the decrease in the surface energy of the droplet, which suppresses the formation of WZ islands on surface energetic grounds.

II. EXPERIMENTAL RESULTS

Our growth procedure and *in situ* diagnostics are as follows: the GaAs NWs are grown by MBE using EP1203 setup directly on Si(111) substrates. Before introduction into the growth chamber, the substrates are chemically treated in HF (10% in water) for 1 min, and then rinsed in deionized water. The deposition rate of GaAs is set at 1 monolayer per second (ML/s) (~0.28 nm/s), as measured on a separate GaAs(100) substrate by the reflection high-energy electron diffraction (RHEED) oscillation technique. A conventional arsenic source producing As tetramers is used. Before the growth of NWs, the substrate temperature (measured by a calibrated pyrometer) is increased to the desired value within the range 560–630 °C, and is kept constant during the whole growth run. In this temperature window, a native oxide layer on Si(111) substrate looses continuity and openings (i.e., the holes penetrating through the oxide toward the substrate surface) are formed.[33] The surface density of openings depends on the temperature. Above 630 °C, the oxide layer is completely desorbed, as detected by the corresponding transformation of RHEED pattern. After the formation of openings, the Ga flux is supplied to the surface for 5 s while the As shutter is closed. This initiates the formation of Ga droplets in the openings. To ensure the deposition conditions providing the NW growth, the As_4/Ga flux ratio is decreased down to ~0.4. When the As flux is switched on, the NW growth is started after an incubation time. The latter is clearly detected by the transformation of the RHEED pattern and typically amounts to 2–10 s, depending on the temperature. Total growth time is 20 min in all cases. During the NW growth, the RHEED pattern features pronounced three-dimensional spots of cubic ZB phase regardless of the temperature. The spot structure does not change during the whole growth run excluding the very final stage after the Ga shutter is closed. At this stage, the RHEED pattern converts to a mixture of spots resulting from the diffraction from ZB and WZ lattices.

A typical scanning electron microscopy (SEM) image of the sample grown at 590 °C is presented in Fig. 1, where the droplets seated on the tops of the longest NWs are clearly seen. A small fraction of short NWs that do not seem to have the droplets on top will be ignored in the foregoing analysis. Statistical analysis of the SEM images of different samples allowed evaluation of the substrate temperature dependence of the NW length and surface density. It is found that the average length of 1.8–1.9 μm, and the density of ~1

$\times 10^8$ cm^{-2} remain almost constant in the lower temperature range, i.e., from 560 to 600 °C. At higher temperatures, the NW density increases up to $\sim 4 \times 10^8$ cm^{-2} at 630 °C while the length behavior is nonmonotonic, first increasing up to ~ 3 μm at 610 °C and than decreasing down to ~ 2.5 μm at 630 °C. Energy-dispersive x-ray analysis after growth shows that the droplet consists of pure Ga. All NWs have almost uniform diameters of $\sim 70-80$ nm from base to top. These values are lower than the critical diameter for coherent epitaxial growth of GaAs on Si(111) (i.e., 110 nm).[6] The average length of 1.8 μm corresponds to the average NW growth rate of 1.5 nm/s. At a higher temperature of 610 °C, the NW growth rate reaches its maximum at 2.5 nm/s. The observed NW growth rates are 5.4–8.9 times higher than the deposition rate of 0.28 nm/s so that the NW length is much larger than the deposition thickness. This proves the diffusion-induced mode of NW growth with major contributions from the adatom migration to the top, as is usual during MBE.[9,12,19,22,34]

In common with the first-type NWs in Ref. 30, our data clearly show the presence of a Ga droplet on top of most NWs. We therefore propose the following growth mechanism: initial droplets formed in the openings in the absence of an As flux must consist of pure liquid Ga. When the As deposition is started, the growth species are supplied to the droplet by direct impingement and, more importantly, by surface diffusion. The corresponding diffusion fluxes are driven by the difference in chemical potentials on the surface and in the droplet. Rather than being a chemical catalyst as in the MOCVD case, the droplet acts as a material collector.[19] Since stoichiometric GaAs cannot be formed in the liquid volume (because of its low As content), Ga and As are transferred through the droplet to the solid surface (initially Si and then GaAs), where a supersaturated liquid crystallizes in the VLS fashion via 2D nucleation.[18–20] After the steady-state growth mode is achieved, the droplet size and shape remains constant due to a dynamic balance between the GaAs arrival to the droplet and the GaAs sink at the liquid-solid interface.[35] The latter provides continuous building of NW MLs. Effectively, liquid Ga now plays the role of Au in the standard Au-assisted NW growth. As demonstrated by the SEM image in Fig. 1, the contact angles of all droplets after growth are larger than 110°.

The prevalent NW growth direction is [111], however a small fraction of NWs are tilted randomly with respect to the substrate surface. Using SEM, we indexed the sidewall facets against the [110] cleavage planes of the substrate. Regardless of the substrate temperature, the NW cross section is a regular hexagon with six equivalent lateral facets (as shown in the inset of Fig. 1), identified as being of (211) family. Since the facets are of the $(2\bar{1}\bar{1})$ type, there are important considerations with respect to sidewall surface energies, discussed in the next section.

For transmission electron microscopy (TEM) investigations of the crystal structure, the NWs are scraped from the substrate with a scalpel, transferred to holey carbon films and analyzed using a JEOL 2100F TEM operated at 200 kV. Conventional bright-field TEM imaging of the NWs combined with selected area diffraction and phase contrast lattice imaging, is used to identify the crystal structures. The NWs grown at different temperatures were checked for crystal structure, twining, and stacking faults over their entire length, Fig. 2 showing typical TEM images. It was found that the majority of the length of the NWs adopted the ZB phase, but that the region immediately beneath the Ga droplet had the WZ crystal structure [Fig. 3(a), region B], the material having undergone a transition (region C). Indeed the twins, stacking faults, and polytypes associated with WZ-ZB phase instability are better known for the case of the II-VI semiconductors, for which the stabilization energy is generally lower than the III-Vs (see Ref. 36 for a description). Close examination of region C in Fig. 3 shows how the purely ZB part transforms via the introduction of single stacking faults, then narrow twin lamellae, followed by random stacking, the WZ structure with some stacking faults and ultimately the pure WZ phase. As mentioned already, the phase mixing (stacking transition) happens only when the Ga-supplying flux is stopped, and is therefore associated with an abrupt change in growth conditions.

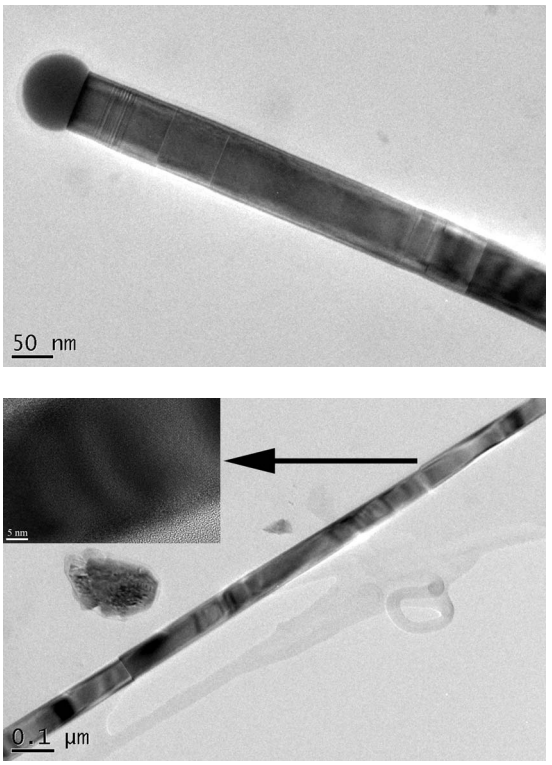

FIG. 2. Multibeam bright-field diffraction contrast TEM images of upper part of a NW terminated by a Ga droplet preceded by a region characterized by planar faults on the (111) growth planes (a) and the main part of a NW showing the general absence of stacking faults and mixed-phase regions. The dark bands are diffraction contrast features (bend contours) that are not associated with stacking disorder (b). High-resolution TEM closeup, shown in the inset, demonstrates pure ZB phase in the NW.

III. MODEL AND DISCUSSION

As discussed previously in Ref. 16, and more recently in Ref. 37, the wire-vapor surface energy of lateral facets γ_{WV} is

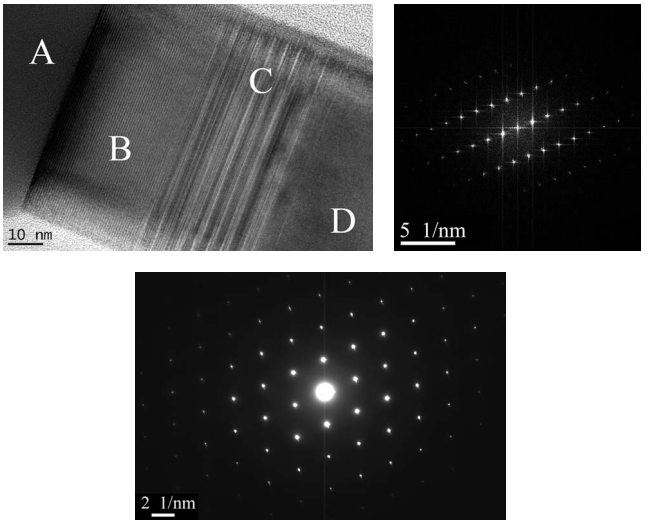

FIG. 3. High-resolution TEM image of upper part of the NW (top left) and corresponding diffraction patterns. Region A—the Ga catalyst, region B—the WZ phase region [the Fourier transform (top right) shows the $(11\bar{2}0)$ WZ zone axis]. In the transition region C, the structure contains twins, and region D has the pure ZB phase [the selected area diffraction pattern in figure (c) shows the (110) ZB zone axis and was acquired from a region far removed from the Ga droplet]. The scales in (top right) and (bottom) are 5 nm^{-1} and 2 nm^{-1}, respectively.

largest for the $(2\bar{1}\bar{1})$ ZB facets so the phase transition to WZ should be most favorable. Estimates in Ref. 37, based on simply counting the density of dangling bonds created by the dissection of crystal by the corresponding vertical planes, give the following values: $\gamma_{WV}=1.73$ J/m^2 for the $(2\bar{1}\bar{1})$ ZB plane, 1.30 J/m^2 for the $(1\bar{1}00)$ WZ plane, and 1.50 for the $(11\bar{2}0)$ WZ plane. Therefore, the "direct" $(2\bar{1}\bar{1})\rightarrow(1\bar{1}00)$ ZB-WZ transition with parallel sidewall planes yields a 25% surface energy gain while the "indirect" $(2\bar{1}\bar{1})\rightarrow(11\bar{2}0)$ ZB-WZ transition (associated with 30° angular rotation of the entire NW) yields a 13% gain. Therefore, the ZB-WZ phase transition should be most favored for the case of $(2\bar{1}\bar{1})$ facets.

To explain the observed ZB phase of our NWs, we use the nucleation model of Ref. 18, illustrated in Fig. 4. We assume that the NW growth is mediated by the nucleation of 2D islands, where the formation of nuclei having the WZ orientation on a ZB NW template can happen at the liquid-solid interface (C) [Fig. 4(a)] or at the TL [Fig. 4(b)]. In the latter case, a fraction x of WZ nucleus perimeter is in contact with the vapor. Under the assumption of phase-independent surface energy of lateral solid-liquid interface (i.e., γ_{SL}=const for the ZB and WZ nuclei because of the close atomic environments on the surface around the two types of nuclei[18,19]), the formation enthalpy of a monolayer island with surface area A and perimeter P is given by[19]

$$\Delta G = -\left[\Delta\mu - \psi - \frac{2\gamma_{LV}(\Omega_S - \Omega_L)\sin\beta}{R}\right]\frac{Ah}{\Omega_S} + \Gamma Ph. \quad (1)$$

Here, $\Delta\mu$ is the chemical potential in the liquid phase with respect to ZB solid state, ψ is the stacking-fault energy (ψ =0 for ZB and $\psi=\psi_{WZ}>0$ for WZ nucleus), Ω_S and Ω_L are the elementary volumes in the solid and liquid phase, respectively, R is the NW radius, β is the contact angle of the droplet, and h is the height of a ML. The R-dependent term in Eq. (1) accounts for the Gibbs-Thomson (GT) effect. The effective lateral surface energy Γ is written down as

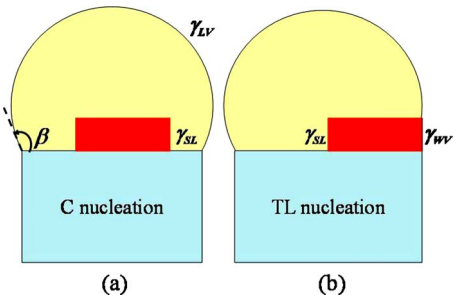

FIG. 4. (Color online) Nucleation of a 2D island in the C TL positions. Nucleation at the TL position eliminates a part of preexisting liquid-vapor interface with effective energy $\gamma_{LV}\sin\beta$ and replaces it with the wire-vapor interface having energy γ_{WV}.

$$\Gamma = (1-x)\gamma_{SL} + x(\gamma_{WV} - \gamma_{LV}\sin\beta). \quad (2)$$

Here, γ_{SL} is the surface energy of lateral solid-liquid interface, γ_{LV} is the surface energy of liquid droplet, $x=0$ for the C nucleation, and $x>0$ for the TL nucleation. Since $\Gamma_C=\gamma_{SL}$ is identical for ZB and WZ nuclei, the GT term (at $\Omega_s\cong$const for the both phases) is phase independent and $\psi_{WZ}>0$, the C nucleation always occurs preferentially in the ZB phase. The formation of a WZ layer therefore necessarily requires the TL nucleation.[18] This happens only when the TL nucleation barrier for a WZ nucleus is lower than the C one. From Eqs. (1) and (2), the difference $\Delta G_{TL}-\Delta G_C$ equals

$$\Delta G_{TL} - \Delta G_C = xPh(\gamma_{WV} - \gamma_{SL} - \gamma_{LV}\sin\beta). \quad (3)$$

A given nucleus therefore tend to form at the TL provided that[18]

$$\Delta\gamma = \gamma_{WV} - \gamma_{SL} - \gamma_{LV}\sin\beta < 0, \quad (4)$$

where the sidewall surface energy γ_{WV} should be taken for WZ sidewall planes.

For further estimates, we use the values of surface energies of Ref. 19: $\gamma_{WV}=1.3$ J/m^2, $\gamma_{SL}=0.59$ J/m^2, and $\gamma_{LV}=1.0$ J/m^2. According to Refs. 38 and 39, the surface energy of pure liquid Au equals 1.145 J/m^2 at temperature $T_m=1065$ °C, and the surface energy of pure liquid Ga amounts to 0.711 J/m^2 at temperature $T_m=30$ °C. As in Ref. 40, we account for the decrease in liquid surface energy at higher temperatures using the linear interpolation formula

$$\gamma_{LV}(T) = \gamma_{LV}(T_m) - c(T - T_m), \quad (5)$$

where T is the growth temperature. With this approximation and the known coefficients c [$c=2.0\times10^{-4}$ $J/(m^2\times°C)$ for Au and 7.0×10^{-5} $J/(m^2\times°C)$ for Ga],[38,39] we arrive at $\gamma_{LV}=1.24$ J/m^2 for pure Au and $\gamma_{LV}=0.67$ J/m^2 for pure Ga at typical MBE growth temperature $T=590$ °C. The value of $\gamma_{LV}=1.0$ J/m^2 therefore corresponds to approximately 40% Ga concentration in the Au-Ga alloy during the

growth. After growth, all our droplets have contact angles between 110° and 125°(the contact angles should be even larger during the growth when the droplets contain more Ga and some As). With these β, we obtain $\Delta\gamma$ from −0.23 to −0.11 J/m^2 for the Au-assisted growth so Eq. (4) would be safely satisfied and the TL nucleation of WZ nuclei would be indeed preferable. In our Ga-catalyzed growth, under standard assumption of a low concentration of As in the droplet,[18,19] the liquid-vapor surface energy is decreased to its value for pure liquid Ga, $\gamma_{LV}=0.67$ J/m^2. This yields positive $\Delta\gamma$ form 0.08 to 0.16 J/m^2 so that the TL nucleation becomes energetically suppressed. Changing the catalyst to a lower surface-energy liquid makes the substitution of its surface to a more energetically costly wire-vapor interface unfavorable. It should be noted, however, that our estimates lead to rather small positive values of $\Delta\gamma$. This may qualitatively explain the onset of twinning defects and WZ phase at the end of growth, where the droplet decreases in size and consequently the contact angle changes as some Ga is emptied into the solid NW phase.

It is noteworthy that whenever the TL nucleation condition given by Eq. (4) is broken, the crystal structure should be less dependent on the liquid supersaturation and the factors influencing the latter, such as the temperature and arsenic flux. The arsenic pressure can, however, change the surface energy of sidewall facets γ_{WV} but this dependence is completely unknown for the WZ NWs. As regards the temperature behavior, our experiments (performed at fixed As_4/Ga flux ratio) reveal pure ZB phase in the entire growth window from 560–630 °C, where we are able to form the NWs by the self-catalyzed growth procedure described hereinabove. Our nucleation model was aimed to identifying the major effect of a lower surface energy of growth catalyst, not yet to give a complete description of the complex interplay of the two phases, including the observed phase mixing upon the growth termination.

IV. CONCLUSIONS

To summarize, we have demonstrated the Au-free, self-catalyzed MBE growth of GaAs NWs having the pure ZB structure on Si(111) substrates. The unexpected phase purity is attributed to the substitution of the growth catalyst from the conventional liquid Au-Ga alloy to pure liquid Ga, whose surface energy is much lower and therefore suppress the TL nucleation. Overall, since the necessary condition for the WZ phase formation involves surface energies, an appropriate choice of the growth catalyst and/or the vapor environment around the droplet can provide a powerful method for the fabrication of pure ZB NWs. This is important for the monolithic integration of chemically pure and stacking-fault-free III-V NWs on silicon. Whenever the TL nucleation becomes energetically unfavorable, ZB crystal structure should become less dependent on the growth conditions and the diameter. We now plan to use the self-catalyzed MBE growth for other NWs of III-V compounds and to investigate their crystal structure from the viewpoint of the obtained results. To this end, the existing nucleation models[18–20,25] are effectively single component and therefore do not include the influence of group V element neither on the liquid phase supersaturation nor on the surface energies. We intend to develop a self-consistent NW growth model to account for these effects.

ACKNOWLEDGMENTS

This work was partially supported by the Russian Federal Agency for Science and Innovation (Contract No. 02.740.11.0383), scientific programs of Russian Academy of Sciences and few grants of Russian Foundation for Basic Research, and also by FP7 EU project POLALAS.

*Corresponding author; cirlin@beam.ioffe.ru

[1] W. Lu and C. M. Lieber, Nature Mater. **6**, 841 (2007).
[2] B. J. Ohlsson, M. T. Björk, M. H. Magnusson, K. Deppert, and L. Samuelson, Appl. Phys. Lett. **79**, 3335 (2001).
[3] R. S. Wagner and W. C. Ellis, Appl. Phys. Lett. **4**, 89 (1964).
[4] F. Glas, Phys. Rev. B **74**, 121302(R) (2006).
[5] L. C. Chuang, M. Moewe, S. Crankshaw, C. Chase, N. P. Kobayashi, and C. Chang-Hasnain, Appl. Phys. Lett. **90**, 043115 (2007).
[6] G. E. Cirlin, V. G. Dubrovskii, I. P. Soshnikov, N. V. Sibirev, Yu. B. Samsonenko, A. D. Bouravleuv, J. C. Harmand, and F. Glas, Phys. Status Solidi (RRL) **3**, 112 (2009).
[7] D. E. Perea, J. E. Allen, S. J. May, B. W. Wessels, D. N. Seidman, and L. J. Lauhon, Nano Lett. **6**, 181 (2006).
[8] A. I. Persson, M. W. Larsson, S. Stengstrom, B. J. Ohlsson, L. Samuelson, and L. R. Wallenberg, Nature Mater. **3**, 677 (2004).
[9] J. C. Harmand, G. Patriarche, N. Péré-Laperne, M.-N. Mérat-Combes, L. Travers, and F. Glas, Appl. Phys. Lett. **87**, 203101 (2005).
[10] K. A. Dick, K. Deppert, T. Martensson, S. Mandl, L. Samuelson, and W. Seifert, Nano Lett. **5**, 761 (2005).
[11] I. P. Soshnikov, G. E. Cirlin, A. A. Tonkikh, Yu. B. Samsonenko, V. G. Dubrovskii, V. M. Ustinov, O. M. Gorbenko, D. Litvinov, and D. Gerthsen, Phys. Solid State **47**, 2213 (2005).
[12] M. Tchernycheva, L. Travers, G. Patriarche, J. C. Harmand, G. E. Cirlin, and V. G. Dubrovskii, J. Appl. Phys. **102**, 094313 (2007).
[13] C.-Y. Yeh, Z. W. Lu, S. Froyen, and A. Zunger, Phys. Rev. B **46**, 10086 (1992).
[14] M. I. McMahon and R. J. Nelmes, Phys. Rev. Lett. **95**, 215505 (2005).
[15] R. Leitsmann and B. Bechstedt, J. Appl. Phys. **102**, 063528 (2007).
[16] V. G. Dubrovskii and N. V. Sibirev, Phys. Rev. B **77**, 035414 (2008).
[17] T. Akiyama, K. Sano, K. Nakamura, and T. Ito, Jpn. J. Appl. Phys. **45**, L275 (2006).
[18] F. Glas, J. C. Harmand, and G. Patriarche, Phys. Rev. Lett. **99**, 146101 (2007).
[19] V. G. Dubrovskii, N. V. Sibirev, J. C. Harmand, and F. Glas,

Phys. Rev. B **78**, 235301 (2008).
[20] J. Johansson, L. S. Karlsson, K. A. Dick, J. Bolinsson, B. A. Wacaser, K. Deppert, and L. Samuelson, Cryst. Growth Des. **9**, 766 (2009).
[21] V. G. Dubrovskii, N. V. Sibirev, G. E. Cirlin, A. D. Bouravleuv, Yu. B. Samsonenko, D. L. Dheeraj, H. L. Zhou, C. Sartel, J. C. Harmand, G. Patriarche, and F. Glas, Phys. Rev. B **80**, 205305 (2009).
[22] H. Shtrikman, R. Popovitz-Biro, A. Kretinin, and M. Heiblum, Nano Lett. **9**, 215 (2009).
[23] J. Johansson, K. A. Dick, P. Caroff, M. E. Messing, J. Bolinsson, K. Deppert, and L. Samuelson, J. Phys. Chem. C **114**, 3837 (2010).
[24] M. Moewe, L. C. Chuang, V. G. Dubrovskii, and C. Chang-Hasnain, J. Appl. Phys. **104**, 044313 (2008).
[25] H. J. Joyce, J. Wong-Leung, O. Gao, H. Hoe Tan, and C. Jagadish, Nano Lett. **10**, 908 (2010).
[26] K. A. Dick, P. Caroff, J. Bolinsson, M. E. Messing, J. Johansson, K. Deppert, R. L. Wallenberg, and L. Samuelson, Semicond. Sci. Technol. **25**, 024009 (2010).
[27] X. Ye, H. Huang, X. Ren, Y. Yang, J. Guo, Y. Huang, and Q. Wang, Chin. Phys. Lett. **27**, 046101 (2010).
[28] H. Huang, X. Ren, X. Ye, J. Guo, Q. Wang, Y. Yang, S. Cai, and Y. Huan, Nano Lett. **10**, 64 (2010).
[29] D. Spirkoska, J. Arbiol, A. Gustafsson, S. Conesa-Boj, F. Glas, I. Zardo, M. Heigoldt, M. H. Gass, A. L. Bleloch, S. Estrade, M. Kaniber, J. Rossler, F. Peiro, J. R. Morante, G. Abstreiter, L. Samuelson, and A. Fontcuberta i Morral, Phys. Rev. B **80**, 245325 (2009).
[30] F. Jabeen, V. Grillo, S. Rubini, and F. Martelli, Nanotechnology **19**, 275711 (2008).
[31] W. Wei, X-Y. Bao, C. Sosi, Y. Ding, Z-L. Wang, and D. Wang, Nano Lett. **9**, 2926 (2009).
[32] S.-G. Ihn, J.-I. Song, T.-W. Kim, D.-S. Leem, T. Lee, S.-G. Lee, E. K. Koh, and K. Song, Nano Lett. **7**, 39 (2007).
[33] N. Wang, Y. Cai, and R. Q. Zhang, Mater. Sci. Eng. R. **60**, 1 (2008).
[34] V. G. Dubrovskii, G. E. Cirlin, I. P. Soshnikov, A. A. Tonkikh, N. V. Sibirev, Yu. B. Samsonenko, and V. M. Ustinov, Phys. Rev. B **71**, 205325 (2005).
[35] V. G. Dubrovskii, N. V. Sibirev, G. E. Cirlin, J. C. Harmand, and V. M. Ustinov, Phys. Rev. E **73**, 021603 (2006).
[36] K. Durose, in *Narrow Gap II-VI Compounds for Optoelectronic and Electromagnetic Applications*, edited by P. Capper (Chapman and Hall, London, 2007), pp. 239–250.
[37] N. V. Sibirev, M. A. Timofeeva, A. D. Bolshakov, M. V. Nazarenko, and V. G. Dubrovskii, Phys. Solid State **52**, 1428 (2010).
[38] J. J. Jasper, J. Phys. Chem. Ref. Data **1**, 841 (1972).
[39] G. J. Janz, National Bureau of Standards Report No. NSRDS-NBS 28, 1969 (unpublished).
[40] V. G. Dubrovskii, N. V. Sibirev, G. E. Cirlin, I. P. Soshnikov, W. H. Chen, R. Larde, E. Cadel, P. Pareige, T. Xu, B. Grandidier, J.-P. Nys, D. Stievenard, M. Moewe, L. C. Chuang, and C. Chang-Hasnain, Phys. Rev. B **79**, 205316 (2009).